Particle physics phenomenology with python 3: $e^- + \bar{\nu}_e \rightarrow e^- + \bar{\nu}_e$ scattering in the fermi theory

I. Domínguez Jiménez, R. J. Hernández-Pinto, and D. F. Rentería-Estrada
Facultad de Ciencias Físico-Matemáticas, Universidad Autónoma de Sinaloa,
Avenida de las Américas y Boulevard Universitarios, Ciudad Universitaria, 80000, Culiacán, Sinaloa, México.
e-mail: isadoji@uas.edu.mx; roger@uas.edu.mx; davidrenteria.fcfm@uas.edu.mx

Received 17 February 2020; accepted 7 March 2020

In this work, we develop an algorithm based on Python 3 to compute the theoretical prediction of the electron and electron anti-neutrino scattering cross-section using two different numerical methods: *i)* Riemann sums and *ii)* Monte Carlo integration. We compare the precision among these two methods and the theoretical result. Besides, the theoretical prediction is compared with the result obtained with MadGraph 5, which is commonly used to provide theoretical predictions for the LHC. With this project, we would like to encourage students to use programming languages as a tool for the study of new physics.

Keywords: High energy physics phenomenology; new computational tools.

PACS: 13.90.+i; 02.70.-c; 07.05.Tp

DOI: https://doi.org/10.31349/RevMexFisE.17.150

1. Introduction

When we immerse ourselves in physics, quickly, we realize that the fundamental tool to explain the laws of nature is mathematics. Besides, when we try to do extensive calculations, manual computation becomes an exhaustive work, and the probability to make mistakes grows very fast. Therefore, to pursuit such computations, it is important to make use of proper software. Technological advances allow us to perform many calculations with the help of automated software but, in general, they do not provide us with the full information *step by step*.

In theoretical physics, we often find ourselves with laborious computations, for example, the calculation of scattering cross-sections among particles within the framework of Quantum Field Theories. In this document, we present a method to perform the calculation of the differential scattering cross-section between an electron and its corresponding electron anti-neutrino through a numerical algorithm implemented in Python 3 [1]. This article is organized as follows: a general review of the weak interactions, the Fermi Theory, and the analytical computation of $e^-\bar{\nu}_e \rightarrow e^-\bar{\nu}_e$ is presented in Sec. 2; in Sec. 3, the results of the implementation of the process in Python 3 and MadGraph 5 [2] are shown. And finally, in Sec. 4 we present our perspectives and conclusions.

2. Weak interactions

In this section, we explain the main properties of leptons and we introduce the Fermi theory, which was the first model that attempted to describe weak interactions. Furthermore, we present the mathematical framework that is used to compute the total scattering cross section in the $e^- + \bar{\nu}_e \rightarrow e^- + \bar{\nu}_e$ process.

2.1. Lepton family

Leptons are fundamental particles that interact through weak and electromagnetic forces. They are fundamental particles that can be considered as point-like objects. As they possess spin $1/2$, due to the Pauli exclusion principle, they must obey the Dirac equation. This differential equation will be presented in a forthcoming section, but it is important to mention that it describes the kinematical behavior of leptons and quarks.

Leptons are grouped into three families, each one containing a particle with electric charge -1 (e^-, μ^- and τ^-), and its corresponding neutrino without an electric charge, (ν_e, ν_μ, and ν_τ). Furthermore, both particles have an antiparticle. Table I shows the masses of the six known leptons. In this work, we consider only the first family, (e^- and $\bar{\nu}_e$), but it can be extended to other families.

These elementary particles are produced and measured in different kinds of processes. For instance, neutrino and electron anti-neutrino are produced in beta decays of radioactive elements. They are also created largely from solar fusion processes. It is worth mentioning that the theoretical description of neutrino masses is under investigation. The Standard Model (SM) of particles is written in such a way that neutrinos are massless particles; however, this conception

TABLE I. Leptons and its properties [3].

Particle	Antiparticle	Mass (GeV)
e^-	e^+	0.511×10^{-3}
ν_e	$\bar{\nu}_e$	$< 15 \times 10^{-6}$
μ^-	μ^+	105.7
ν_μ	$\bar{\nu}_\mu$	< 0.19
τ^-	τ^+	1777
ν_τ	$\bar{\nu}_\tau$	< 18

is not consistent with experimental observations. Thus, the community is searching for SM extensions such that neutrinos possess a mass different from zero and its possible implications on future measurements. Nowadays, the measurement of neutrino masses, in particular for electron antineutrino, is a major challenge from the experimental and theoretical points of view. On the other hand, regarding the stability of leptons, the electron is a stable particle; however, muon and tau leptons decay into other leptons as,

$$\mu^- \to e^- + \bar{\nu}_e + \nu_\mu, \tag{1}$$

$$\tau^- \to \mu^- + \bar{\nu}_\mu + \nu_\tau. \tag{2}$$

These decay processes are allowed by the weak interaction, the same interaction responsible for the beta decay.

2.2. Beta decay

Nowadays, we know that among all known atomic nuclei, less than 12 % are stable. Particles that constitute unstable atomic nuclei decay by emitting alpha or beta particles. An alpha particle is a helium nucleus with total spin equal to zero and, a beta particle can be an electron (β^-) or a positron (β^+), depending on the type of beta decay. There are three kinds of beta decay processes:

$$n \to p + e^- + \bar{\nu}_e, \qquad \beta^- \text{ decay}\,, \tag{3}$$

$$p \to n + e^+ + \nu_e, \qquad \beta^+ \text{ decay}\,, \tag{4}$$

$$p + e^- \to n + \nu_e, \qquad e^- \text{capture}\,. \tag{5}$$

The β^- decay occurs whenever the mass of the original neutral atom is greater than the mass of the final atom. The β^+ decay can be presented when the atomic mass of the original atom is at least two electron masses greater than the mass of the final atom. Finally, electron capture happens when the original atomic mass is greater than the final atomic mass.

A phenomenological description of the beta decay must take into account that electrons and neutrinos do not exist in the nucleus before its disintegration[i]. It means that electromagnetic and strong interactions remain invariant (symmetric) under parity transformation; however, the beta decay breaks the invariance under parity. In this kind of process, neutrinos always have their spin pointing in the opposite direction to its velocity, and, anti-neutrinos have their spin parallel to its velocity [4]. All these facts were modeled by Fermi, without knowing the existence of the weak force, in the so-called Fermi's interaction or Fermi theory of beta decay.

2.3. The Fermi theory of beta decay

In 1934, Fermi postulated that the beta decay process must be described by a Hamiltonian in which the particles are interacting among them, through the so-called Fermi four-fermion interactions. These interactions contain the four free particle wave functions involved in beta decay (neutron, proton, electron, and neutrino),

$$H_F = H_n^0 + H_p^0 + H_e^0 + H_\nu^0 + H_{int}\,, \tag{6}$$

where H_F is called Fermi's Hamiltonian, H_n^0, H_p^0, H_e^0, and H_ν^0 are the free hamiltonians for neutron, proton, electron, and antineutrino; and H_{int} is the interaction hamiltonian that can be written as,

$$H_{int} = \sum_i C_i \int d^3x (\bar{u}_p \widehat{O}_i u_n)(\bar{u}_e \widehat{O}_i u_\nu)\,, \tag{7}$$

where u_n and u_ν are the neutron and neutrino wave functions. The bars on the proton and electron wave functions are defined as $\bar{u}_p = u_p^\dagger \gamma^0$ and $\bar{u}_e = u_e^\dagger \gamma^0$, the $\widehat{O}_i$ are operators which characterize the beta decay and are weighted by the constants C_i. In practice, we can neglect neutrino masses, and the electron mass is also small if we compare it with the dispersed kinetic energy in the beta decay. This implies that the theory must be relativistic and therefore, the wave functions must be solutions of the free particle Dirac equation [5],

$$\left(\imath\gamma^\mu \frac{\partial}{\partial x^\mu} - m_k\right) u_k(x) = 0\,, \tag{8}$$

where γ^μ are the Dirac matrices, and $k = \{p, n, e, \nu\}$. These matrices are defined as,

$$\gamma^i = \gamma^0 \alpha^i, \qquad i = 1, 2, 3\,, \tag{9}$$

where,

$$\gamma^0 = \begin{pmatrix} \mathbf{1}_{2\times2} & \mathbf{0}_{2\times2} \\ \mathbf{0}_{2\times2} & -\mathbf{1}_{2\times2} \end{pmatrix}, \quad \alpha^i = \begin{pmatrix} 0 & \sigma_i \\ \sigma_i & 0 \end{pmatrix}. \tag{10}$$

and σ_i are the so-called Pauli matrices.

The interaction term in Eq. (6) is modeled by a current-current point-like interaction, which is well known from electrodynamics. To consider the most general interaction term, the current is written as $\bar{u}_p \widehat{O}_i u_n$. In Table II, we enlist the different operators $\widehat{O}_i$ and their properties under Lorentz transformations of the current $\bar{\Psi}\widehat{O}_i\Psi$. In any case, the operator $\widehat{O}_i$ must be a 4×4 spin matrix. Also, the differential operators can be reduced to constant 4×4 matrices, since we are dealing with plane wave functions. Explicitly, Eq. (8) allows us to express the differential operators $\imath\gamma^\mu \partial u_k(x)/\partial x^\mu$ as $m_k u_k(x)$ [6].

TABLE II. Elemental fermion transition operators.

$\widehat{O}_i$	Transformation property	Number of matrices
1	Scalar	1
γ^μ	Vector	4
$\sigma^{\mu\nu} = \frac{\imath}{2}[\gamma^\mu, \gamma^\nu]$	Tensor	6
$\gamma^\mu\gamma_5$	Axial vector	4
$\gamma_5 = \imath\gamma^0\gamma^1\gamma^2\gamma^3$ $= -\imath\gamma_0\gamma_1\gamma_2\gamma_3$	Pseudoscalar	1

Parity violation in beta decay suggests that the allowed interactions in Eq. (6) can only be,

$$H_{\rm int} = \frac{G_F}{\sqrt{2}} \int d^3x\, \bar{u}_p(x)\gamma_\alpha(C_V + C_A\gamma_5)u_n(x) \times \bar{u}_e(x)\gamma^\alpha\left(1-\gamma_5\right)u_{\nu_e}(x)\,, \quad (11)$$

where $\bar{u}_e(x)\gamma^\alpha\left(1-\gamma_5\right)u_{\nu_e}(x)$ is the leptonic contribution, with $C_A/C_V = -1.255 \pm 0.006$ [7], and C_A and C_V are the axial and vector contribution of the nuclear coupling, respectively. G_F is called the Fermi constant. It is important to notice that Lorentz invariance of the total Hamiltonian requires both, vector and axial operators. See Table II. Finally, for the study performed in this work, we emphasize that the vector nuclear coupling constant is often related to the Fermi constant of beta nuclear decay ($G_\beta = G_F C_V$) [8]. The experimental determination of the Fermi constant started with the measurements of the muon decay [9]. After the introduction of the Higgs mechanism in the SM, it is found that [10]:

$$\frac{G_F}{\sqrt{2}} = \frac{g^2}{8M_W^2}\,, \quad (12)$$

where g is the coupling constant of the weak interaction, and $M_W = 80.387 \pm 0.016$ GeV is the mass of W-boson [11,12]. The current measurement of the Fermi constant in the electroweak model is $G_F = 1.1663787(6) \times 10^{-5}\text{GeV}^{-2}$ [13].

2.4. $e^- + \bar{\nu}_e \to e^- + \bar{\nu}_e$ scattering in the Fermi theory

In this work, we are interested in the process $e^- + \bar{\nu}_e \to e^- + \bar{\nu}_e$ in the framework of the Fermi Theory. As it has been argued in the previous sections, this process can be studied by a contact four fermion interaction given by H_F. The Feynman diagram associated with this process is shown in Fig. 1.

To describe the $e^- + \bar{\nu}_e \to e^- + \bar{\nu}_e$ scattering process, it is important to know the wave functions of all particles. The wave functions for the electron and the electron anti-neutrino are described by the solutions of the Dirac Eq. (8). The incoming and outgoing wave functions are given in terms of Dirac spinors as,

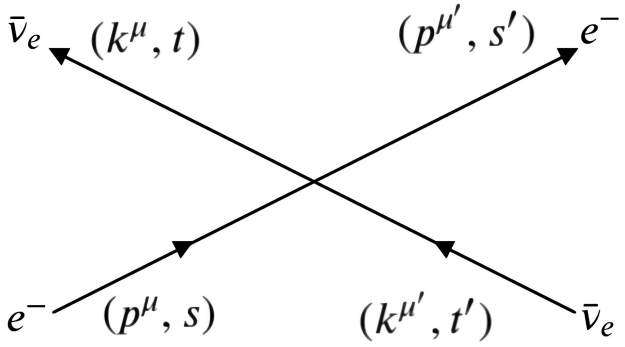

FIGURE 1. Feynman diagram for $e^-\bar{\nu}_e \to e^-\bar{\nu}_e$ scattering within the Fermi theory.

$$|\Psi_{\rm In}\rangle = \begin{cases} u_e(x) = \left(2p^0V\right)^{-\frac{1}{2}} u_e\left(\mathbf{p},s\right)\mathrm{e}^{-ip_\mu x^\mu} \\ u_{\bar{\nu}_e}(x) = \left(2k^0V\right)^{-\frac{1}{2}} v_{\bar{\nu}_e}\left(\mathbf{k},t\right)\mathrm{e}^{ik_\mu x^\mu} \end{cases} \quad (13)$$

and

$$|\Psi_{\rm Out}\rangle = \begin{cases} u_e(x') = \left(2p'^0V\right)^{-\frac{1}{2}} u_e\left(\mathbf{p}',s'\right)\mathrm{e}^{-ip'_\mu x^\mu} \\ u_{\bar{\nu}_e}(x') = \left(2k'^0V\right)^{-\frac{1}{2}} v_{\bar{\nu}_e}\left(\mathbf{k}',t'\right)\mathrm{e}^{ik'_\mu x^\mu} \end{cases} \quad (14)$$

where p, k are the momenta of the incoming e^- and $\bar{\nu}_e$, and p' and k' are the momenta of the outgoing e^- and $\bar{\nu}_e$, respectively. In the same spirit, s and t represent the spin of the incoming e^- and $\bar{\nu}_e$ and s' and t' represent the spin of the outgoing e^- and $\bar{\nu}_e$ and finally, V is the volume factor of the phase-space integration domain. Taking into account the Feynman rules [18] of the diagram in Fig . 1, we compute the elementary transition matrix element by means of the Fermi Golden Rule, which it is given by

$$S\left(\bar{\nu}_e e^- \to \bar{\nu}_e e^-\right) = -\imath\frac{G_F}{\sqrt{2}}\left(2\pi\right)^4 \times \frac{\delta^{(4)}\left(p'+k'-p-k\right)}{\sqrt{16V^4\,k_0\,p_0\,k'_0\,p'_0}}\,\mathcal{M}\,, \quad (15)$$

where the invariant amplitude $\mathcal{M}$ is,

$$\mathcal{M} = \bar{u}_{\nu_e}\left(\mathbf{k},t\right)\gamma_\mu\left(1-\gamma_5\right)u_e\left(\mathbf{p},s\right) \times u_e\left(\mathbf{p}',s'\right)\gamma^\mu\left(1-\gamma_5\right)\bar{u}_{\nu_e}\left(\mathbf{k}',t'\right)\,. \quad (16)$$

Then, the differential cross-section per unit of the phase-space volume of two particles in the final state can be computed as,

$$d\sigma = \left(J_{12}\rho_2\,V\,T\right)^{-1}|S|^2\,V\,\frac{d^3p'}{(2\pi)^3}\frac{d^3k'}{(2\pi)^3}\,, \quad (17)$$

where the density of particle two is given by $\rho_2 = V^{-1}$ and, with a proper normalization of the wave function, the incoming current corresponding to particle one takes the form,

$$J_{12} = \frac{\sqrt{(p_1\cdot p_2)^2 - m_1^2\,m_2^2}}{p_1^0\,p_2^0\,V}\,. \quad (18)$$

Besides, the angular distribution of the cross-section in the center of the mass system can be written as,

$$\frac{d\bar{\sigma}}{d\Omega}\left(\bar{\nu}_e e^- \to \bar{\nu}_e e^-\right) = V\int\frac{d^3p'}{(2\pi)^3}V\int\frac{d|\mathbf{k}'|}{(2\pi)^3}|\mathbf{k}'|^2 \times \frac{1}{2}\sum_{s,s',t,t'}\frac{|S|^2k^0p^0V}{(k\cdot p)V^{-1}(VT)} = \frac{G_F^2}{2\pi^2}\frac{1}{16(k\cdot p)} \times \int\frac{d^3p'}{2p'_0}\int\frac{|\mathbf{k}'|^2d|\mathbf{k}'|}{2k'_0}\delta(p'+k'-p'-k') \times \frac{1}{2}\sum_{s,s',t,t'}|\mathcal{M}|^2\,. \quad (19)$$

The invariant amplitude squared averaged over spins can be computed using standard Dirac algebra, and we find,

$$\sum_{s,s',t,t'} |\mathcal{M}|^2 = \mathrm{Tr}[\gamma_\alpha(1-\gamma_5)(\not{p}+m_e)\gamma_\beta(1-\gamma_5)\not{k}] \times \mathrm{Tr}[\gamma^\alpha(1-\gamma_5)\not{k}'\gamma^\beta(1-\gamma_5)(\not{p}'-m_e)] \,. \quad (20)$$

In the process studied in this document, the anti-neutrino with momentum $k^{\mu\prime}$ and spin t' represents an "incoming" particle with negative energy, while the incoming anti-neutrino with momentum k^μ and spin t is an "outgoing" particle. Also, the electron with momentum $p^{\mu\prime}$ and spin s' represents an outgoing particle, and the electron labeled with momentum p^μ and spin s represents an incoming particle. Furthermore, we can write the differential cross-section distribution in terms of two kinematical variables: *i)* the scattering angle θ measured with respect to the center of the mass system and *ii)* the Mandelstam variable $s = (p_0+k_0)^2$. Thus, we find that the invariant amplitude squared averaged over spins can be written as,

$$\sum_{s,s',t,t'} |\mathcal{M}|^2 = 256\,(k\cdot p)\,(p'\cdot k) = \frac{256}{16}\left(s-m_e^2\right)^2 \times \left[1+\frac{m_e^2}{s}+\left(1-m_e^2\right)\cos\theta\right]^2 . \quad (21)$$

The remaining factors of the Eq. (19) take the form,

$$(k\cdot p) = \frac{1}{2}\left(s-m_e^2\right), \quad (22)$$

and

$$\int \frac{d^3p'}{p_0'}\int \frac{|\mathbf{k}'|^2 d|\mathbf{k}'|}{k_0'}\delta(p'+k'-p'-k') = \int \frac{d^3p'}{p_0'}\int_0^\infty dk_0'\,k_0'\,\delta(p'+k'-p'-k') = \frac{\left(s-m_e^2\right)}{2s} . \quad (23)$$

Inserting the results of Eqs. (21), (22) and (23) in Eq. (19), we find,

$$\frac{d\bar{\sigma}}{d\Omega}\left(\bar{\nu}_e e^- \to \bar{\nu}_e e^-\right) = \frac{G_F^2}{16\pi^2}s\left(1-\frac{m_e^2}{s}\right)^2 \times \left[1+\frac{m_e^2}{s}+\left(1-\frac{m_e^2}{s}\right)\cos\theta\right]^2 . \quad (24)$$

This process and the explicit theoretical prediction is explained and developed in several textbooks [19], as well as the rules for computing the reaction of two particles in the initial state to $n-$particles in the final state within the framework of quantum field theories.

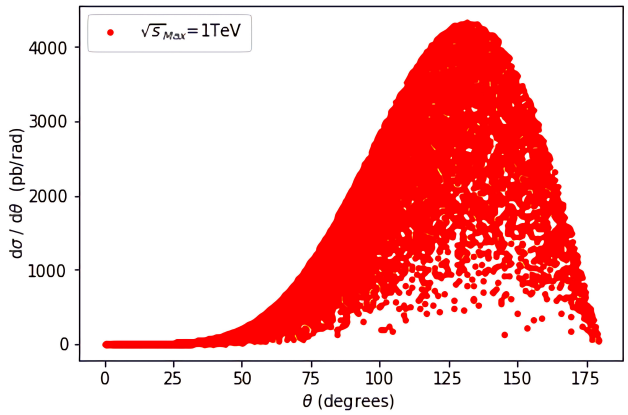

FIGURE 2. The differential cross section for the process $e^-\bar{\nu}_e \to e^-\bar{\nu}_e$ as a function of the dispersion angle in the Fermi theory.

3. Results

In this section, we present a phenomenological analysis for the $\bar{\nu}_e e^- \to \bar{\nu}_e e^-$ process. To compute the total cross-section, we solve numerically Eq. (19). To do so, we generate 20,000 random events, and we impose the constraint that the center of mass energy is smaller than 1 TeV. The generated events are shown as a distribution in Fig. 2. To compare with available codes, we need to convert GeV^{-2} to pico barn (pb) units; the conversion factor is 1 pb = 2.56819×10^{-9} GeV^{-2}. The distribution in Fig. 2 shows that the largest number of events have an angular dispersion between 100 and 150 degrees.

To compute the total cross-section, we obtain the area under the curve from the distribution showed in Fig. 2 by two different methods: *a)* Riemann sums and *b)* Monte Carlo method. Then, we compare both methods and, finally, we contrast the theoretical calculation with the results provided by MadGraph 5 [2], a program that simulates the collisions at the LHC. The Riemann sums method consists of choosing the maximum points from the distributions and sum the areas produced by these points. In the Monte Carlo method, we make a linear regression to build a curve that is fitted to the

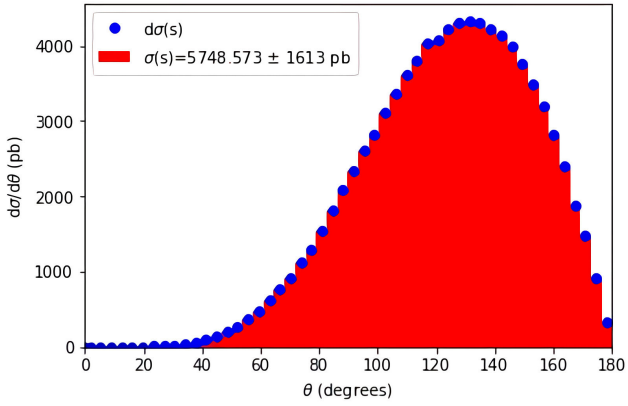

FIGURE 3. Differential cross section of $e^-\bar{\nu}_e \to e^-\bar{\nu}_e$ in the Fermi theory estimated with Riemann sums at $\sqrt{s} = 1$ TeV.

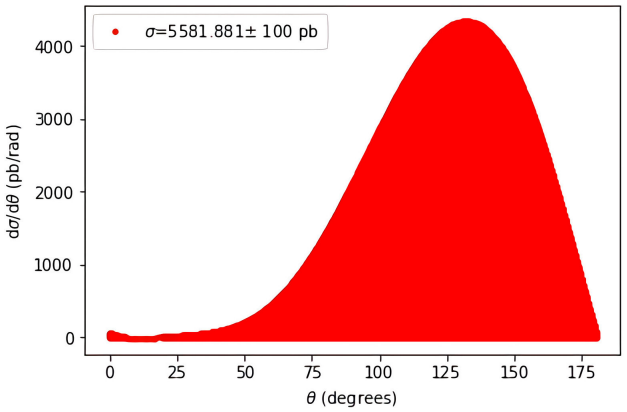

FIGURE 4. Differential cross section of $e^-\bar{\nu}_e \to e^-\bar{\nu}_e$ in the Fermi theory estimated with a Monte Carlo method at $\sqrt{s} = 1$ TeV.

maximum points. Then, we compute the area under this curve by generating random points, and finally, we estimate the area under the curve. Then, we use 50 points to estimate the cross section distribution shown in Fig. 2, through Riemann sums. In Fig. 3, we obtain that the total cross-section $\sigma(s) = 5748.573 \pm 1613$ pb by Riemann sums method.

Now, we turn into the Monte Carlo method. In this case, we make a linear regression over the maximum points of the dispersion shown in Fig. 2. This curve is named *envelope*. Once we obtain the envelope, we use the Monte Carlo method to compute the total cross section described previously. The result obtained by the Monte Carlo method is $\sigma(s) = 5581.881 \pm 100$ pb. It is important to point out that we have generated the same number of events for the Monte Carlo method as for the Riemann sums.

To compare both methods, we compute Eq. (19) with `Mathematica` [20], which includes the necessary libraries to solve Eq. (19) easily. The results are shown in Fig. 5. Therefore, the theoretical prediction obtained with `Mathematica` is $\sigma(s) = 5577.178$ pb at $\sqrt{s} = 1$ TeV.

Up to now, the total cross-section has been estimated from a purely theoretical point of view. To conclude our analysis, we use MadGraph 5 [2], which is a Monte Carlo event generator that simulates events at the LHC energies; however,

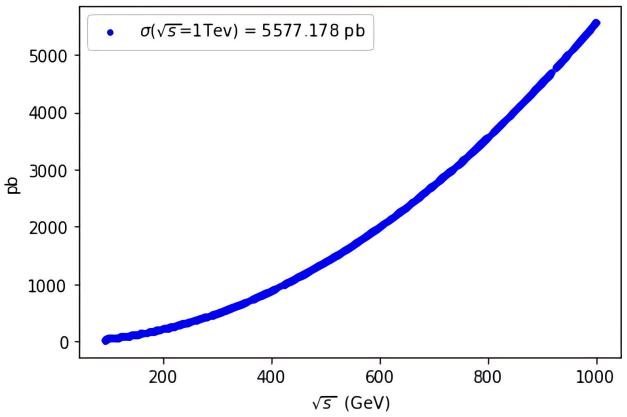

FIGURE 5. Evolution of the total cross section for the process $e^-\bar{\nu}_e \to e^-\bar{\nu}_e$ in the Fermi theory with Mathematica.

TABLE III. Total cross section for $e^-\bar{\nu}_e \to e^-\bar{\nu}_e$ estimated with MadGraph 5 [2].

Run	Collider (GeV)	Cross Section (pb)	Events
run 1	500 × 500	5.378 ± 0.005	1000
run 2	500 × 500	5.365 ± 0.0045	1000
run 3	500 × 500	5.377 ± 0.0048	1000

it can be also set the conditions for the $e^-\bar{\nu}_e \to e^-\bar{\nu}_e$ process. Figure 3 shows the result for 10,000 generated events. The simulation shows that the cross section is 5.373 ± 0.0048 pb at $\sqrt{s} = 1$ TeV.

4. Conclusions

In this work, we have presented the computation of the total cross section of $e^-\bar{\nu}_e \to e^-\bar{\nu}_e$ with Python 3. We implemented a code based on Python 3 to compute the total cross-section; furthermore, we use two different methods for the calculation, *1)* the Riemann sums and *2)* the Monte Carlo method. Figure 3 and Fig. 4 indicate the areas studied by the two methods. Computing the cross-section with the Riemann sums method, we obtained a total cross-section of $\sigma(s) = 5748.573 \pm 1613$ pb, while by using the Monte Carlo method, we find that the total cross section is $\sigma(s) = 5581.881 \pm 100$ pb. To compare the two results, we scan the total cross section from 0 to 1 TeV by using `Mathematica`; and we obtained $\sigma(s) = 5577.178$ pb. This implies that the method by Riemann sums gives a calculation error of of 2.98 %, while the method Monte Carlo provides an error of 0.08%.

Besides the numerical analysis, we compare our results with MadGraph 5, an LHC simulator which we tuned for computing $e^-\bar{\nu}_e \to e^-\bar{\nu}_e$ at $\sqrt{s} = 1$ TeV. With the use of MadGraph 5, we find that the total cross-section is $\sigma(s) = 5.373 \pm 0.0048$ pb. The total cross-section computed by MadGraph is around 10^3 times smaller than the theoretical predictions; this is because Madgraph 5 has kinematical cuts in some variables while we are computing the full cross-sections with no cuts. In other words, the phase-space available for the integral is dramatically reduced in MadGraph 5. To take into account kinematical cuts, we need to perform the same computation but in terms of pseudorapidity and transverse momentum as it is for the LHC. This is a program to be done in a future analysis in Python 3.

Finally, in this work, we showed that Python 3 is a powerful tool for computing observables in High Energy Physics Phenomenology. The algorithm implemented in this work can help us to understand the process $e^-\bar{\nu}_e \to e^-\bar{\nu}_e$ within the Fermi Theory. The aim of this work is also to motivate students to use and generate new tools in other programming languages, as Python 3, for the study of physics problems.

The codes written in Python 3 to compute the differential cross-section with both methods are available in: https://github.com/DavidRenteria/PhenomenologyWithPython3-electronantineutrino

Acknowledgments

Support for this work has been received in part by Consejo Nacional de Ciencia y Tecnología grant number A1-S-33202 and the COST Action CA16201 PARTICLEFACE.

i. Fermi developed the theory of the beta decays through a perturbation of the "Golden Rule" by introducing the weak interaction.

1. J. Kiusalaas, Numerical methods in engineering with Python 3 (Cambridge University Press, 2013).
2. J. Alwall, R. Frederix, S. Frixione, *et al. J. High Energ. Phys*. (2014) . https://doi.org/10.1007/JHEP07(2014)079
3. Particle Data Group, *Phys. Rev. D*. **98** (2018) 36. https://doi.org/10.1103/PhysRevD.98.030001
4. E. J. Konopinski, *Revs. of Mod. Phys*. **15** (1943) 209. https://doi.org/10.1103/RevModPhys.15.209
5. E. Fermi, *Ric. Sci*. **4** (1933) 491. https://doi.org/10.1098/rspa.1928.0023
6. P. A. M. Dirac, *Proc. Roy. Soc. Lond.* **117** (1928) 610. https://doi.org/10.1098/rspa.1928.0023
7. J. C. Hardy and I. . Towner, *Nucl. Phys*. **254** (1975) 221. https://doi.org/10.1016/0370-2693(78)90161-2
8. S. D. Aristizabal, *Phys. Rev.* **98** (2018) 075018. https://doi.org/10.1103/PhysRevD.98.075018
9. C. M. S. Collaboration, *Phys. Lett. Sec. B.* **768** (2019) 124. https://doi.org/10.1016/j.physletb.2017.02.061
10. P. Fayet, *Nucl. Phys. B*. **90** (1975) 104. https://doi.org/10.1016/0550-3213(75)90636-7
11. D. B. Chitwood, *Phys. Rev. Lett.* **99** (2007) 032001. https://doi.org/10.1103/PhysRevLett.99.032001
12. Particle Data Group, *Phys. Lett.* **239** (1990) III.1. https://doi.org/10.1016/0370-2693(91)91762-K
13. Particle Data Group, *Phys. Lett*. **98** (2019) 030001. https://doi.org/10.1103/PhysRevD.98.030001
14. C. G. Callan Jr, *Phys. Rev. D.* **2** (1970) 1541. https://doi.org/10.1103/PhysRevD.2.1541
15. M. E. Machacek *Phys. Rev. D.* M. T. Vaughn, *Nucl. Phys. B.* **222** (1983) 83. https://doi.org/10.1016/0550-3213(83)90610-7
16. D. R. T. Jones, *Phys. Rev. D.* **25** (1982) 581. https://doi.org/10.1103/PhysRevD.25.581
17. N. G. Deshpande, E. Keith and P. B. Pal, *Phys. Rev. D.* **47** (1993) 2892. https://doi.org/10.1103/PhysRevD.47.2892
18. D. Griffiths, *Introduction to elementary particles*, Wiley (John Wiley and Sons, 1987).
19. W. Greiner, and B. Müller, *Gauge theory of weak interactions*, 3th ed. (Springer-Verlag, Berlin, 1996), pp. 88.
20. https://www.wolframalpha.com/calculators/integral-calculator